The Effects of the Model Scale and Mach Number on the Aerodynamic Characteristics of one six-blade Propeller

Liu Zhang, Li-tao Liu, Hui Zhang, Hong Chen

Low Speed Aerodynamics Institute, China Aerodynamics Research and Development Center, Mianyang, 622762, China

Corresponding author: *lzh2607@126.com*

Abstract: The viscous flow fields around a propeller with six blades as well as its aerodynamic characteristics have been numerically derived with unsteady N-S equations based on the MRF (Multiple Reference Frames). The computational results agree well with the experimental data, implying that the methodology has enough accuracy for the simulation of the flow field. Further, the variations of aerodynamic characteristics of the propeller with the model scale and Mach number are obtained with different model scales, ranging from 1:1 to 1:15, at fixed values of the advance ratio λ and blade angle ϕ. The results show that the thrust coefficient and torque coefficient may not decrease with the Reynolds number considering the combined effects of both the free stream speed and model scale, which induce opposite change trends in the propeller efficiency. Moreover, the Mach number and the model scale have little influence on the distribution shape of dimensionless velocities in three directions (r, θ, x) and the effect domain of slipstream after the propeller.

Keywords: Mach Number, Model Scale, Propeller, Aerodynamic Characteristics.

1   Introduction

The flow similarities of one six-blade propeller include geometric similarity, kinematic similarity and dynamic similarity[1-3]. The kinematic similarity between two different physical processes requires that the advance ratios (i.e. the Strouhal number), which represent the kinematic characteristics of the two processes, are identical. The dynamic similarity include Reynolds number, Mach number and Froude number similarity[3]. In the wind tunnel experiments on propeller slipstream effects, the scaled model is usually used considering the constraint of wind tunnel size and expenditure. Further, the incoming flow velocity in the wind tunnel is far lower than that in flight test, leading to the discrepancy of the experimental Reynolds number with flight Reynolds number. The discrepancy in the Reynolds number as well as other similarity parameters may induce disadvantageous effect on the usability of the wind tunnel test data.

A great amount of researches has been devoted to the effects of Reynolds number on the aerodynamic characteristics of flight vehicles with the purpose of revealing the effect mechanism of Reynolds number and utilizing fully the wind tunnel test data under the lower Reynolds number condition. It is shown that the lift–to-drag ratio could change remarkably with the variations of Reynolds number[4-5]. Such behavior is worth being examined cautiously as the change of Reynolds number is achieved only by means of changing the model scale and density of fluid in these studies. While for the propeller test in low speed wind tunnel, the power of electrical machine in use can't

meet the demand of lifting incoming flow velocity substantially, and the investigation on the effects of Reynolds number from the point of changing incoming flow velocity is lacking[6-7].

Thus, we focus on the effects of Mach number (i.e. the incoming flow velocity) on the aerodynamic characteristics of the propeller which are compared with those of model scale, and neglect the way of changing density of fluid as it is rarely seen in low speed wind tunnel. The unsteady finite-volume RANS equations are solved to obtain the aerodynamic characteristics of the propeller based on the MRF in which grid is generated to have multi-block structure[8-12], and the thrust coefficient and torque coefficient of the propeller are also calculated. The computational results may provide some beneficial suggestions on how to improve the propeller experiment technique in low speed wind tunnel and how to modify the wind test data to the flight condition.

2   Model and Mesh

The propeller we studied has six blades with the diameter value of 4m and the hub-to-radius ratio of 0.2. The nonlinear twist angle is 30˚ from the tip to root of the blade. The X axis is rotation axis, which is parallel with the free stream, and the YOZ plane is the rotating face. Viewing from the positive of X axis, the blades rotate in the clockwise direction. A large amount of tests on the aerodynamic performance of this type of propeller have been conducted in some low speed wind tunnels in China aerodynamics research and development center with different advance ratios and free stream velocities.

In the construction process of computational meshes based on MFR, the rotational subzone which contains the propeller and the stationary one were separated. Also, when the rotational subzone is chosen, we make sure that this area not just wrap the blades, but also leave enough space for the growth of the grid within boundary layer. For the 1:6 model, the radius of the rotational subzone is 350mm, and its axial length is 105mm, as shown in figure 1.

In order to keep the consistency of meshes between different models, which is needed for the comparison of computational results, we select the mesh for 1:6 model as standard and obtain the meshes for other scaled models by zooming in or out standard mesh. Figure 2 shows the surface mesh of the propeller. In order to obtain the complicated flow phenomenon, we arrange a large number of grids in the rotation area and the wake flow area after the propeller, especially at the tip of the blade. There are 3.8 million cells in the rotational subzone and 1.6 million cells in the stationary subzone, respectively.
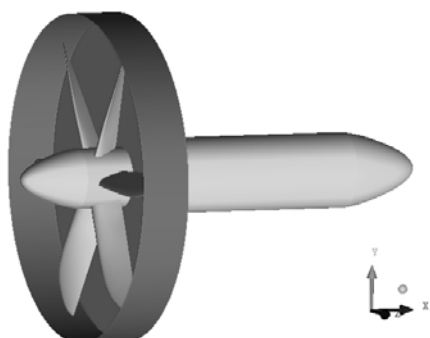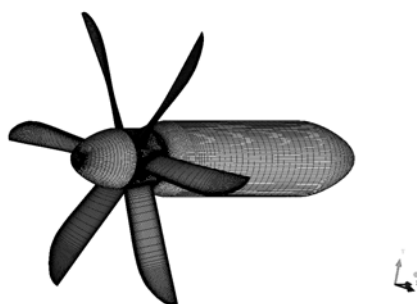

Figure 1: The propeller model.   Figure 2: Surface mesh.

3   Problem formulation and computation states

A. Problem formulation

The viscous flow fields around a propeller with six blades as well as its aerodynamic characteristics have been numerically derived with unsteady N-S equations, which can be written as follows:

$$\frac{\partial}{\partial t}\iiint_{\Omega} Q\,dV + \iint_{\partial\Omega} F(Q)\bullet\vec{n}\,dS = \iint_{\partial\Omega} G(Q)\bullet\vec{n}\,dS$$.

A second order upwind scheme was used for space diffusion, and an implicit LU-SGS scheme was employed for time marching. The computation is carried out using $k-\omega$ SST model for the simulation of fully developed turbulent flow.

B. Computation states

The contents of computation states are listed in table 1. The free stream velocities for model scales of 1:6 and 1:15 are 35m/s and 40m/s, which are fixed according to the parameters of the engine and the rotation speed of 1075rev/min under the same advance ratio defined in formula (1) with the model scale of 1:1. The flow fields around the propellers with model scales from 1:6 to 1:15 at fixed advance ratio, blade angle and Mach number are simulated and compared with each other. The Reynolds number for the flow after one propeller is calculated through formula (2).

$$\lambda = \frac{V}{nD} \tag{1}$$

$$\mathrm{Re} = \frac{\rho l\sqrt{V^2 + \left(0.5r\omega D\right)^2}}{\mu} \tag{2}$$

where:

D diameter of the propeller(m);

l chord length at the 70% section of blade(m);

n rotation speed(rev/min);

r the radius at the 70% section of blade (m);

V free stream velocity (m/s);

ρ air density （kg/m^3）;

ω angular speed （rad/s）;

μ air viscosity (pa.s).

Table1: Computation states

Model scale	Velocity(m/s)	Advance ratio	Rotate speed (rev/min)	Reference length (m)	Reynolds number
1:1	58.6	0.818	1075	0.396	2.66x10^6
1:1	53.7	0.75	1075	0.396	2.59x10^6
1:1	49.6	0.692	1075	0.396	2.52x10^6
1:6	58.6	0.818	6450	0.066	4.43x10^5
1:6	53.7	0.75	6450	0.066	4.32x10^5
1:6	49.6	0.692	6450	0.066	4.2x10^5
1:6	35	0.818	3850	0.066	2.65x10^5
1:6	35	0.75	4200	0.066	2.81x10^5
1:6	35	0.692	4550	0.066	2.97x10^5
1:15	58.6	0.818	16125	0.0264	1.77x10^5
1:15	53.7	0.75	16125	0.0264	1.73x10^5
1:15	49.6	0.692	16125	0.0264	1.68x10^5
1:15	40	0.818	11000	0.0264	1.21x10^5
1:15	40	0.75	12000	0.0264	1.28x10^5
1:15	40	0.692	13000	0.0264	1.36x10^5

4　Results

A. Mathematical Verification

The computational results are compared with the experiment data to check the accuracy of the computation method for the simulation of the flow field. Figure 3 and Figure 4 give the comparisons of thrust coefficient and torque coefficient between calculation and experiment results, respectively. It is shown that the error of thrust coefficient is less than 3% while that of the torque coefficient less than 2% within the range of the advance ratio from 0.818 to 0.692, implying that the numerical method used for the solution of the flow field is reliable.
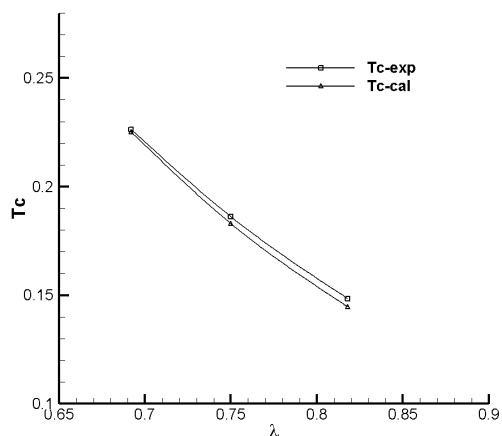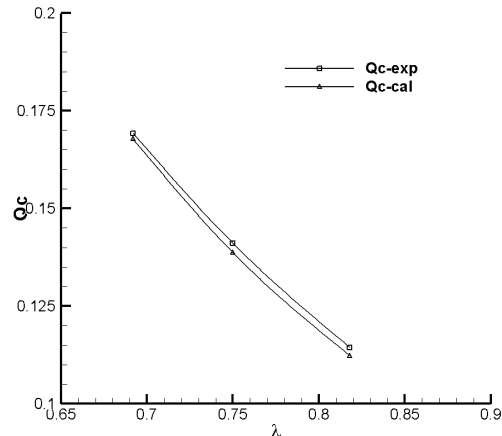

Figure 3: Thrust coefficient comparison.   Figure 4: Torque coefficient comparison.

B. The analysis of aerodynamic forces

The comparison of the propeller thrust coefficients which were calculated with different model scales and incoming velocities is given in figure 5. Further, the variations of torque coefficient and efficiency with the advance ratio are given in figure 6 and figure 7. The mark of Ma(1:1) in these figures means that the computational states are of the same velocity with the model scale of 1:1.

As shown in figure 5, in the cases with fixed model scale, the thrust coefficient decrease with decreasing incoming velocity; while with fixed incoming velocity, the thrust coefficient decrease with decreasing model scale. The change rule of the torque coefficient with model scale and flow velocity is similar to that of the thrust coefficient, as seen from figure 6.

At the advance ratio of 0.818, the thrust coefficient and torque coefficient for model scale of 1:6 at the wind speed of 35m/s (i.e. Re=2.65×10^5) are less than those for model scale of 1:15 at the speed of 58.6m/s (Re=1.77×10^5). This implies that the thrust and torque of the propeller with larger Reynolds number may be smaller than those of the model with smaller Reynolds number. Further, we can also obtain the same conclusion for other advance ratios. Viewing the above results, we can conclude that the way of magnifying the scale of the model without raising the free stream velocity may not leads to the best results for the simulation of flight condition.
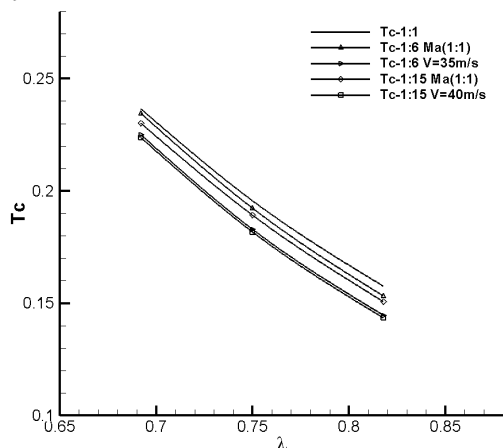

Figure 5: Thrust coefficients with   Figure 6: Torque coefficients with
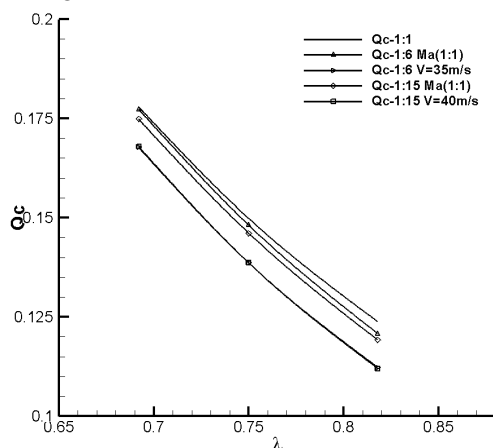different model scales and velocities.   different model scales and velocities.

The efficiencies of the single propeller with different advance ratio, Mach number and model scale have been compared in figure 7. From formula (3) we can find that the efficiency of the single propeller is proportional to the ratio of thrust coefficient to torque coefficient at the same advance ratio. For the same Mach number, the Reynolds number and the aerodynamic forces of the propeller (thrust and torque) decrease with the decrease of the model scale, and the thrust decreases more quickly than the torque, thus the efficiency of the propeller is reduced. While for the same model scale, the Reynolds number and the aerodynamic forces of the propeller decrease with the decrease of Mach number, and the torque decreases more obviously than the thrust, so the efficiency of the propeller is increased. The model scale and the Mach number of incoming flow have opposite effect trends in the efficiency of the propeller.

$$\eta = \frac{TV}{P} = \frac{0.5Tc\rho V^2 SV}{Cq\rho V^2 D^3 2\pi n} = \frac{TcSV}{Cq\,4\pi nD^3} = k\,\frac{Tc}{Cq}\,\lambda \propto \frac{Tc}{Cq}$$

(3)

where:

η efficiency of the propeller;

T thrust force of the propeller(N);

P the power of the propeller;
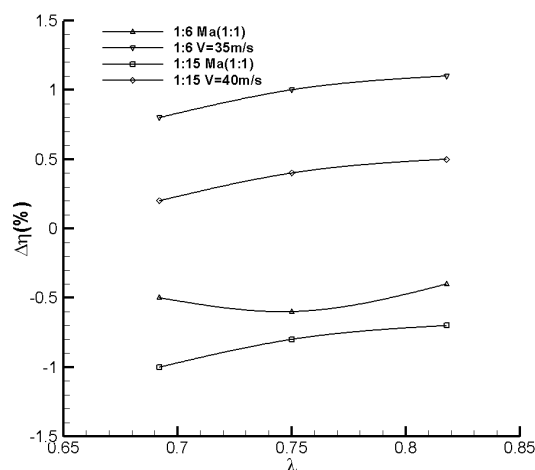
k constant.

Figure 7: Efficiencies with different model scales and flow velocities

C. Analysis of the Flow Field

We use the same time step, during which the blade can rotate 3.6 degrees, to resolve the equations. The phase angles of the blades were kept constant for all computational cases, which could guarantee the comparison between different cases reasonable.

Figure 8，figure 9 and figure 10 give the distribution shapes of dimensionless velocities in three directions (axial, radial and tangential velocities) in the flow field after 1:1 and 1:6 propeller models with the incoming velocity of 58.6m/s and 1:6 model with incoming velocity of 35m/s under the advance ratio of 0.818. Figure 8(a) shows that the axial velocity increases along the downstream direction until the location where the distance from the propeller is 1.7 times the radius, and the dimensionless axial velocity reaches 1.7[8] [13-15]. The dimensionless axial velocity is larger than 1 within the radius of the blade and decrease with the increase of radial coordinate outside the propeller. Figure 8(b) depicts the distribution of radial velocity and indicates that the tube of the slipstream contracts and the radial velocity is of negative value. Figure 8(c) describes the distribution of tangential velocity and it is shown that the maximum velocity is reached at half the radius of the blade and then decrease to zero at the tip of the blade. This means that the area near the root of the blade has larger rotation velocity while the area near the tip of the blade has smaller rotation velocity. This situation is due to nonlinear twist of blades with the twist angle of 30 degree, which makes the angle between the chord line of the root plane of the blade and the rotation plane larger than the blade angle,

5

and the angle between the chord line of the tip plane of the blade and the rotation plane smaller than the blade angle. So the root area of the blade has greater tangential velocity than the tip area of the blade.

Comparing dimensionless velocities in three directions of different sections with different incoming velocities, it is clearly seen that the flow patterns with model scale 1:1 and model scale 1:6 are completely the same, and only differ in the magnitude of the velocity. So it can be concluded that the sizes of the effect domain of the propeller slipstream and flow shapes are similar, and the Mach number and the model scale have little influence on the distribution shapes of the flow structures.
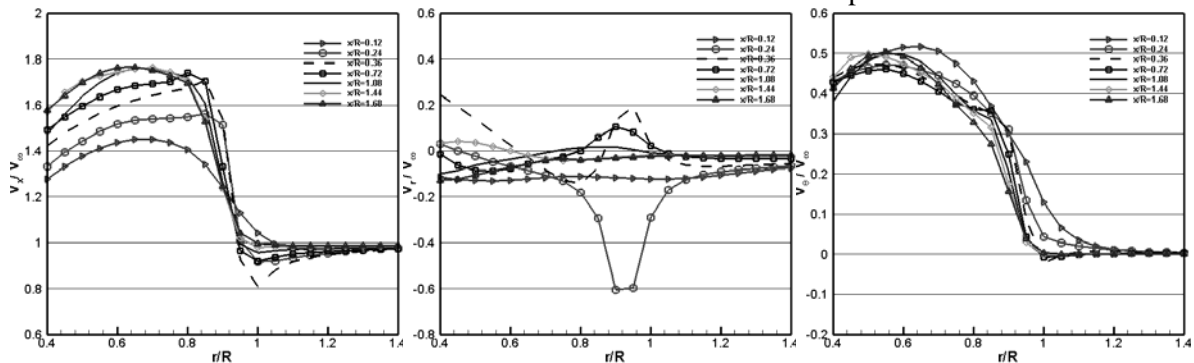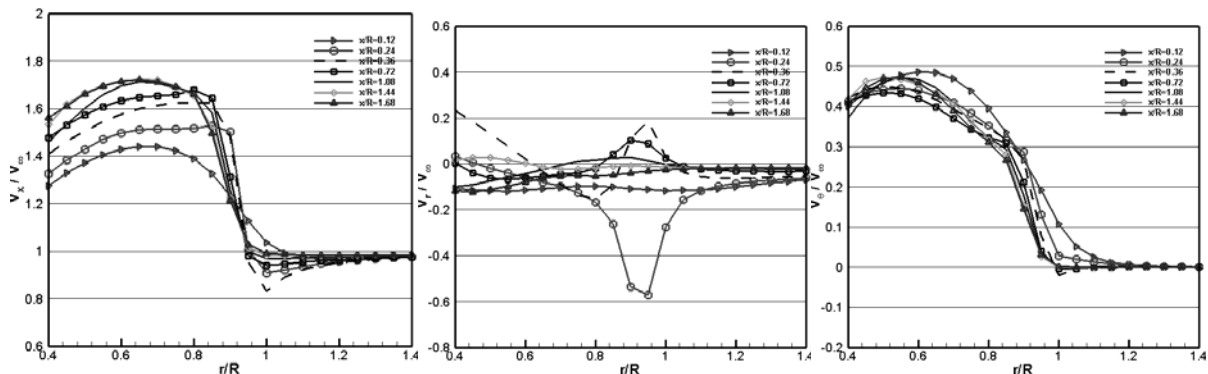

(a) axial velocity distribution   (b) radial velocity distribution   (c) tangential velocity distribution

Figure 8: The dimensionless velocity distributions in three directions in different Cross-sections with λ=0.818 (1:1 model).
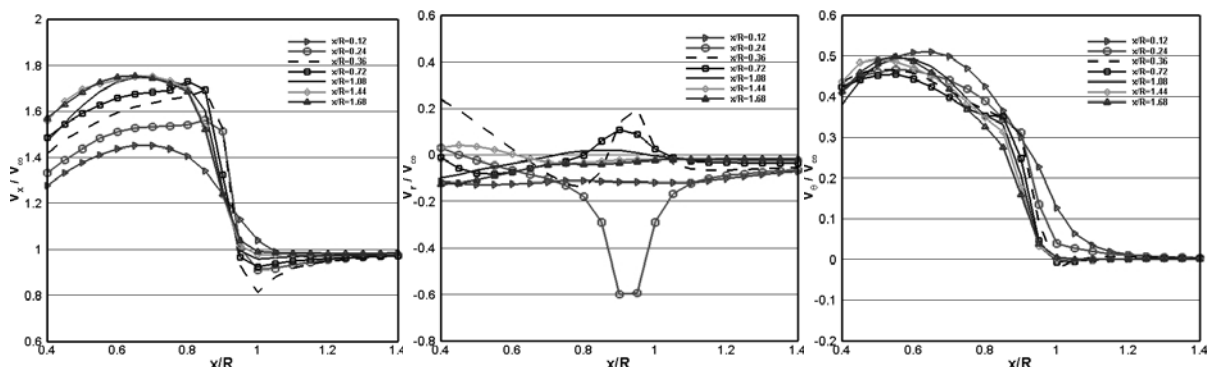
(a) axial velocity distribution   (b) radial velocity distribution   (c) tangential velocity distribution

Figure 9: The dimensionless velocity distributions in three directions in different Cross-sections with λ=0.818 at velocity of 58.6 m/s (1:6 model).

(a) axial velocity distribution   (b) radial velocity distribution   (c) tangential velocity distribution

Figure 10: The dimensionless velocity distributions in three directions in different Cross-sections with λ=0.818 at velocity of 35 m/s (1:6 model).

6

5 Conclusion

The viscous flow fields around one six-blade propeller with different scales have been numerically simulated with unsteady N-S equations. The accuracy of the methodology has been checked through the comparison with the experimental data. Further, we obtain the influence law of the Mach number and model scale on the aerodynamic characteristics of the propeller.

In the low speed wind tunnel, the thrust coefficient and torque coefficient may not decrease with decreasing Reynolds number, only in the cases of fixed model scale or incoming flow Mach number, the two coefficients are seen to decrease with the decrease of the Reynolds number; the efficiency of propeller decreases with decreasing model scale, while it increases with decreasing free stream velocity, implying that the model scale and Mach number induce opposite change trends in the propeller efficiency; the Mach number and the model scale have little influence on the distribution shape of dimensionless velocities in three directions (r,θ,x) and the effect domain of slipstream after the propeller.

References

[1] Yun Qi-lin. Aerodynamic Experiments. [M].Beijing: National Defense Industry Press,1991.

[2] Liu Pei-qing. Air Propeller Theory and Application [M]. Beijing: Beijing University of Aeronautics and Astronautics Press, 2006.

[3] Li Zhou-fu. Wind Tunnel Experiment Technology [M]. Beijing: Aviation Industry Press,2010.

[4] Haines A B, Young A D. Scale Effects on Aircraft and Weapon Aerodynamics[R]. AGARD-AG-323, 1994.

[5] Johnson F T, Tinoco T, Jong Y N. Thirty years of development and application of CFD at Boeing Commerical Airplanr Seattle[R].AIAA2003-3439.

[6] Liu Pei-qing, Ma Rong, Duan Zhong-ze, et al. Ground Wind Tunnel Test Study of the Propeller of Stratospheric Airships[J]. Journal of Aerospace Power, 2011, 26(8): 1775-1784 (in Chinese).

[7] ZHANG Xi-jin, ZHANG Hui. A new method for propeller power simulation test[J]. Journal of Experiments in Fluid Mechanics, 2006,20(2):78-82. (in Chinese).

[8] Zhang Liu, Liu Li-tao, Zhang Rong-ping, et al. Unsteady Numerical Simulation of the Viscous Flow Fields of the Propeller[J]. Journal of Aerospace power, 2013, 28(12):2648-2654 (in Chinese).

[9] Fergal Boyle. Efficient Solution of the Navier-Stokes Equations for Transonic Propeller Flows. AIAA Paper No 2003-4083,2003.

[10] Holmes, D. G., and Tong, S. S. "A Three-Dimensional Euler Solver for Turbo machinery Blade Rows[J]. Journal of Engineering for Gas Turbines and Power, Vol. 107, pp. 258-264, 1985.

[11] Jameson A, Schmidt W, Turkel E. Numerical Solutions of the Euler Equations by Finite Folume Methods Using Runge-Kutta Time Stepping Scheme[R]. AIAA,1981-1259,1981.

[12] Han Zhong-hua. Efficient method for simulation of viscous flows past helicopter rotors and active flow control. Northwestern Polytechnical University. Doctoral dissertation[D].2007.

[13] LI ZHeng-chu, WANG Xun-nian, CHEN Hong, et al. Experimental research of influence of propeller slipstream on wing flow field[J]. Experiments and Measurements

in Fluids Mechanics, 2000,14(2):44-48 (in Chinese) .

[14]   Arne W. Stuermer. Unsteady CFD Simulations of Propeller Installation Effects[R]. AIAA,2006-4969,2006.

[15]   LI Bo, LIANG De-wang, HUANG Guo-ping. Propeller slipstream effects on aerodynamic performance of turbo-prop airplane based on equivalent actuator disk model[J]. Acta aeronautica et astronautica sinica,2008,29(4):845-852 (in Chinese).